

## Electron Cloud Effect and Its Cures in the SuperKEKB Positron Ring

Y. Suetsugu<sup>†</sup>, H. Fukuma, K. Ohmi, M. Tobiyama, K. Shibata

High Energy Accelerator Research Organization (KEK), 305-0801, Tsukuba, Japan

### Abstract

Various countermeasures against the electron cloud effect (ECE) were adopted for the positron ring of SuperKEKB. During Phase-1 commissioning from February to June 2016, however, the ECE was observed, such as a blow up of the vertical beam size. The electron clouds at high beam currents were in the beam pipes at drift spaces in the ring, where antechambers and titanium nitride (TiN) film coating were prepared as countermeasures against ECE. Before starting the next commissioning, permanent magnets and solenoids to generate a magnetic field in the beam direction were attached to the beam pipes as additional countermeasures. Consequently, in the experiment at the end of May during Phase-2 commissioning from March 2018, it was found that the threshold current linear density for exciting ECE increased by a factor of at least 1.5 when compared to that during Phase-1 commissioning.

### INTRODUCTION

The SuperKEKB is an electron-positron collider with asymmetric energies in KEK that aims for an extremely high luminosity of  $8 \times 10^{35} \text{ cm}^{-2} \text{ s}^{-1}$  (Fig.1) [1]. The main ring (MR) consists of two rings, i.e. the high-energy ring (HER) for 7-GeV electrons and the low-energy ring (LER) for 4-GeV positrons. Each ring has four arc sections and four straight sections, as shown in Fig.2.

The single-bunch instability caused by the electron cloud, i.e. the electron cloud effect (ECE), is a serious problem for the SuperKEKB LER [2]. More effective countermeasures than ever before were required. From elaborate simulations, the average density of electrons in the ring should be less than  $\sim 3 \times 10^{11} \text{ m}^{-3}$  in order to avoid the excitation of ECE [3]. Hence, various types of countermeasures were adopted in the SuperKEKB LER, which are summarized in Table 1 [4].



Figure 1: SuperKEKB at KEK Tsukuba campus.

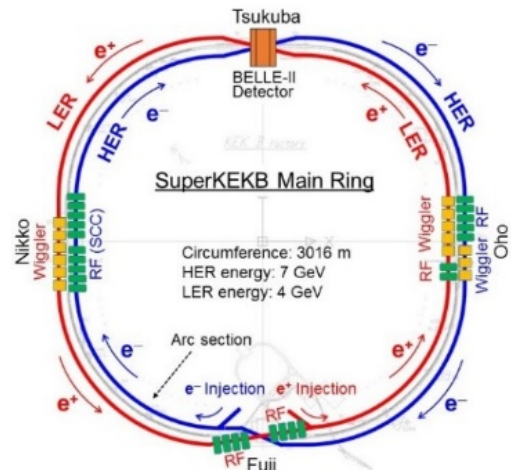


Figure 2: Layout of the SuperKEKB Main Ring (MR). One ring consists of four arc sections and four straight sections.

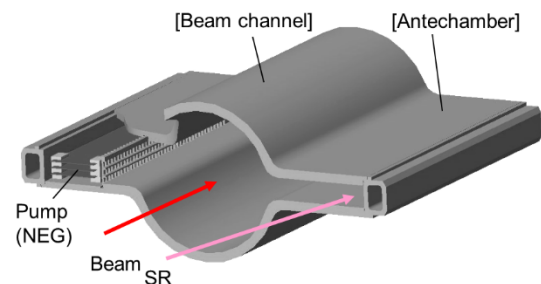


Figure 3: Typical cross section of a beam pipe at arc sections for LER.

An antechamber helps to minimize the effects of photoelectrons, since most of synchrotron radiation (SR) is directly irradiated at the side wall of it. A schematic of a beam pipe with antechamber is shown in Fig. 3. In the high-bunch-current regime, however, secondary electrons play a major role in forming the electron cloud. A magnetic field in the beam direction ( $B$ , [G]) generated by solenoids or permanent magnets around the beam pipe is very effective to suppress the emission of electrons from the inner wall. However, these are available only in the drift spaces (field-free regions) between electromagnets, such as quadrupole and sextupole magnets. Most of the beam pipes for the SuperKEKB LER were made of aluminum (Al) -alloy, and the beam channel was coated with a TiN film to reduce the secondary electron yield (SEY). A grooved surface was adopted for the beam pipes in bending magnets in the arc sections. A grooved surface geometrically reduces the SEY. A TiN film was subsequently applied to the grooved surface. Clearing electrodes were installed in the beam pipes for wiggler magnets instead of the TiN film coating. A clearing electrode absorbs the electrons around the beam orbit by a static electric field. These beam pipes also have

<sup>†</sup> yusuke.suetsugu@kek.jp

Table 1: Countermeasures used to minimize the ECE in the SuperKEKB LER. The circular dots indicate the countermeasures applied for each main section in the ring.

| Sections                      | Length [m] | $n_e$ (circular) [m <sup>-3</sup> ] | Countermeasures   |                   |                           |              |                   | $n_e$ (expected) [m <sup>-3</sup> ] |
|-------------------------------|------------|-------------------------------------|-------------------|-------------------|---------------------------|--------------|-------------------|-------------------------------------|
|                               |            |                                     | Antechamber (1/5) | TiN coating (3/5) | Solenoid ( $B_z$ ) (1/50) | Groove (1/2) | Electrode (1/100) |                                     |
| Drift space (arc)             | 1629       | $8 \times 10^{12}$                  | •                 | •                 | •                         |              |                   | $2 \times 10^{10}$                  |
| Corrector mag.                | 316        | $8 \times 10^{12}$                  | •                 | •                 | •                         |              |                   | $2 \times 10^{10}$                  |
| Bending mag.                  | 519        | $1 \times 10^{12}$                  | •                 | •                 |                           | •            |                   | $6 \times 10^{10}$                  |
| Wiggler mag.                  | 154        | $4 \times 10^{12}$                  | •                 | •*                |                           |              | •                 | $5 \times 10^9$                     |
| Quadrupole and Sextupole mag. | 254        | $4 \times 10^{10}$                  | •                 | •                 |                           |              |                   | $5 \times 10^9$                     |
| RF cav. section               | 124        | $1 \times 10^{11}$                  |                   | •                 | •                         |              |                   | $1 \times 10^9$                     |
| IR                            | 20         | $5 \times 10^{11}$                  |                   | •                 | •                         |              |                   | $6 \times 10^9$                     |
| Total                         | 3016       |                                     |                   |                   |                           |              |                   |                                     |
| Average                       |            | $5.5 \times 10^{12}$                |                   |                   |                           |              |                   | $2.4 \times 10^{10}$                |

\*Except for beam pipes with clearing electrodes.

Abbreviations;

RF cav. section: Beam pipes around RF cavities, IR: Interaction region

$n_e$  (circular): Density of electrons expected for circular beam pipe (copper)

$n_e$  (expected): Density of electrons expected after applying countermeasures

Antechamber: Antechamber scheme, Solenoid: Solenoid winding, but actually applying a magnetic field ( $B_z$ ) in the beam direction

Groove: Beam pipe with grooves, Electrode: Beam pipe with clearing electrodes

antechambers and are made of copper. As a result, approximately 90% of the beam pipes in the ring have the antechambers and TiN coating.

The circular dots in Table 1 indicate the countermeasures applied in each main section in the ring. The density of electrons ( $n_e$  [m<sup>-3</sup>]) expected in the case of circular beam pipes (copper) and those with the above countermeasures are presented in the table. Here, the efficiencies in reducing  $n_e$  for the antechamber scheme, TiN coating, solenoid (i.e.  $B_z$ ), grooved surface, and clearing electrode are assumed to be 1/5, 3/5, 1/50, 1/2, and 1/100, respectively, on the bases of the experimental results obtained thus far [4]. With these all countermeasures, an  $n_e$  [m<sup>-3</sup>] value of approximately  $2 \times 10^{10}$  m<sup>-3</sup> was expected at the designed beam parameters, i.e. a beam current of 3.6 A at a bunch fill pattern of one train of 2500 bunches, with a bunch spacing of 2 RF-buckets (referred to as 1/2500/2RF hereafter). Here, one RF-bucket corresponds to 2 ns. This value of  $n_e$  is sufficiently lower than the threshold density of electrons ( $n_{e,th}$  [m<sup>-3</sup>]), at which the ECE is excited,  $3 \times 10^{10}$  m<sup>-3</sup>. It should be noted that the  $B_z$  at drift spaces were not prepared before Phase-1 commissioning, since the expected beam current was not particularly high during the commissioning, i.e. approximately 1 A at the maximum.

The  $n_e$  around the circulating beam in an Al-alloy beam pipe with antechambers was measured via electron current monitors, which were also used in the previous KEKB experiments [5]. These two electron monitors were set up at the bottom of the beam channel. The voltage applied to the electron collector was 100 V, while that applied to the grid (repeller) varied from 0 V to -500 V. These two electron monitors were attached to the same beam pipe: one in the region with TiN film coating (as in the other typical beam pipes in the ring) and one in the region without the TiN film coating (i.e. bare Al surface). The test beam pipe was

placed in an arc section of the ring. The line density of photons of the synchrotron radiation (SR) is  $1 \times 10^{10}$  photons s<sup>-1</sup> m<sup>-1</sup> mA<sup>-1</sup>. This line density is almost same as the average value of arc sections.

## ECE IN PHASE-1 COMMISSIONING

### First observation

The ECEs, such as a blow up of vertical beam size and a non-linear pressure rise with beam current, were firstly observed during Phase-1 commissioning from a beam current ( $I$  [mA]) of approximately 600 mA at a bunch fill pattern of 1/1576/3.06RF in despite the implementation of the various countermeasures described above [6, 7]. This value of  $I$  corresponds to the current line density ( $I_e$  [mA bunch<sup>-1</sup>]), i.e. the bunch current divided by the bunch spacing, of 0.1–0.12 mA bunch<sup>-1</sup> RF-bucket<sup>-1</sup>. The typical behavior of the average pressure ( $P$  [Pa]) in an arc section divided by  $I$ ,  $P/I$  [Pa mA<sup>-1</sup>], is presented in Fig. 4(a) ([without PM at bellows]). Note that the high  $P/I$  at low  $I$  is due to the effect of base pressures. If the gas load comes from only the photodesorption by the SR, the  $P/I$  should be a constant, since the number of photons is proportional to  $I$ . As shown in Fig. 4(a), however, the  $P/I$  increased with an increase in  $I$ . This increase in  $P/I$  was attributed to the electron-stimulated gas desorption caused by multipactoring of high-density electrons in the beam pipe.

The vertical beam size began to blow up at almost the same  $I$  where the increase in  $P/I$  occurred, as shown in Fig. 4(b) ([without PM at bellows]). The emittance control knob (ECK), which is a tool to adjust the beam emittance using two skew-type quadrupole magnets, was active in this case. However, the behavior of the vertical beam size at  $I \geq 600$  mA was independent of it. Since the  $B_z$  was not applied to beam pipes in Phase-1 commissioning, as described

before, the excitation of the ECE was an undeniable possibility. However, the threshold of beam current for exciting ECE was lower than expected.

A dedicated machine study to investigate the phenomena found that the threshold of  $I_d$  ( $I_{d,th}$  [mA bunch<sup>-1</sup> RF-bucket<sup>-1</sup>]) where the blow up of beam size begins was almost irrespective of the bunch fill pattern as shown in Fig. 5(a). This is a typical characteristic of ECE. The  $I_{d,th}$  was 0.1–0.12 mA bunch<sup>-1</sup> RF-bucket<sup>-1</sup>.

The modes of coupled-bunch instability were also found to be typical modes for ECE due to the electrons in drift spaces. Furthermore, the  $n_e$  was measured at the region without TiN film coating in the test beam pipe. The result at a bunch fill pattern of 1/1576/3.06RF is shown in Fig. 6(a). Note here that high  $n_e$  values at a low  $I$  are not reliable, since the volume used in the calculation of  $n_e$  is so small that the estimation method is no longer valid in principle [5]. The  $n_e$  value was over 20 times higher than the expected  $n_{e,th}$ ,  $\sim 3 \times 10^{11}$  m<sup>-3</sup>, at an  $I$  value of 600 mA, which corresponds to  $I_d \sim 0.12$  mA bunch<sup>-1</sup> RF-bucket<sup>-1</sup>.

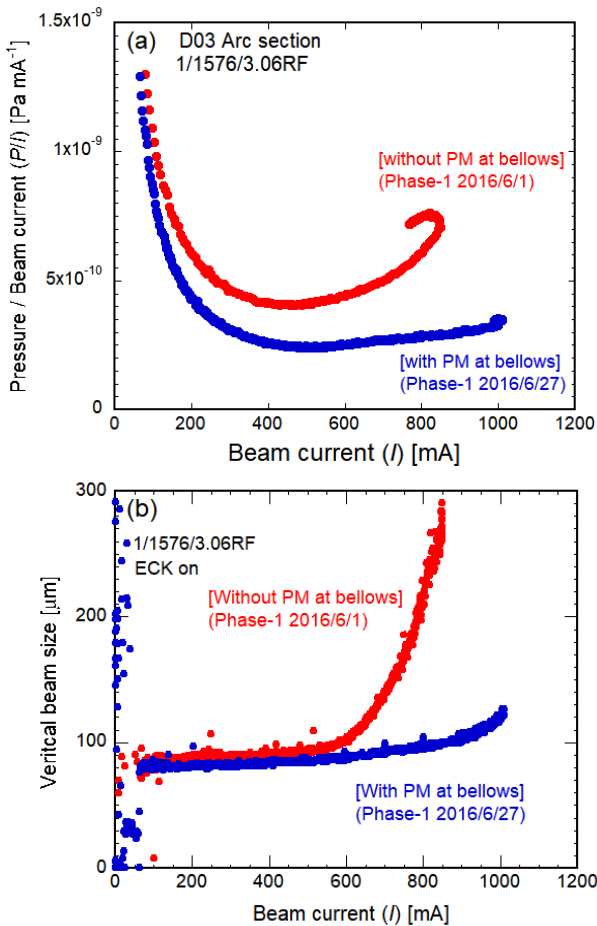


Figure 4: Behaviors of (a) average pressure in an arc section and (b) vertical beam size versus beam current without and with permanent magnets (PM) on Al-alloy bellows chambers for a bunch fill pattern of 1/1576/3.06RF.

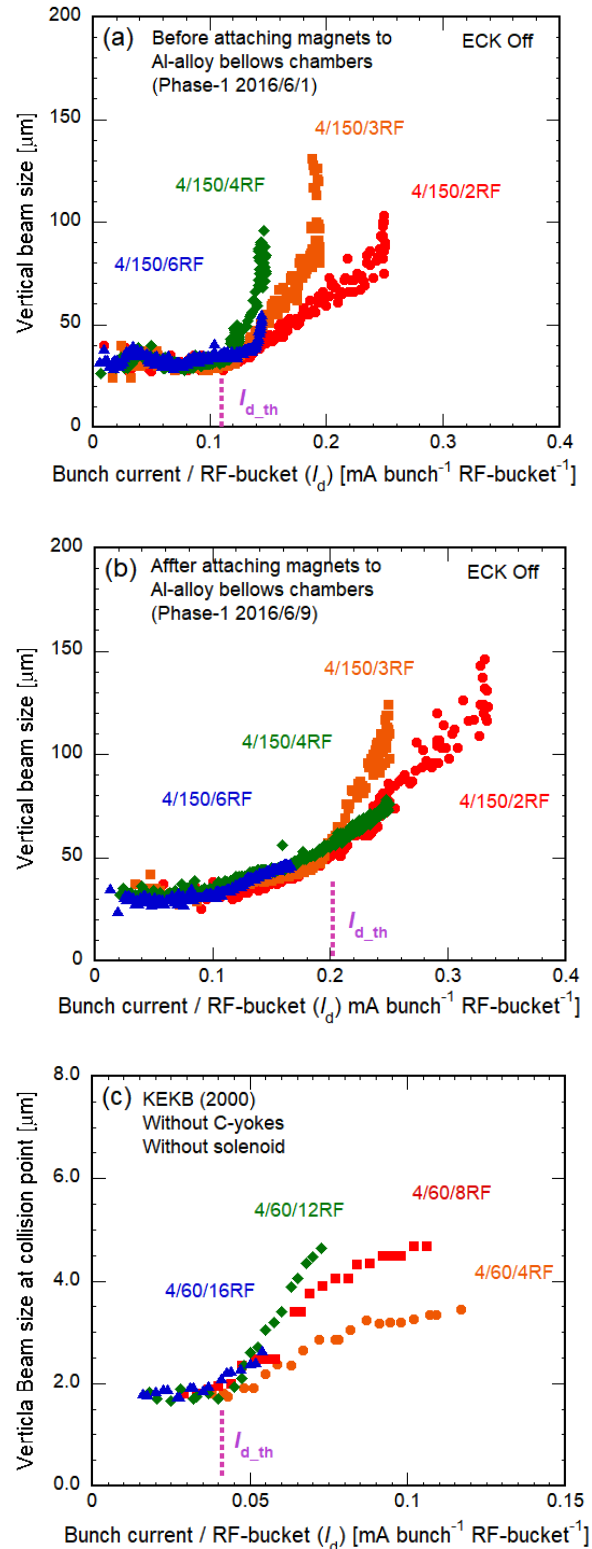


Figure 5: Vertical beam sizes as a function of the current line density ( $I_d$ ) for several bunch fill patterns measured (a) before and (b) after attaching PM units to Al-alloy bellows chambers during Phase-1 commissioning of SuperKEKB, and (c) in the early stage of KEKB era.

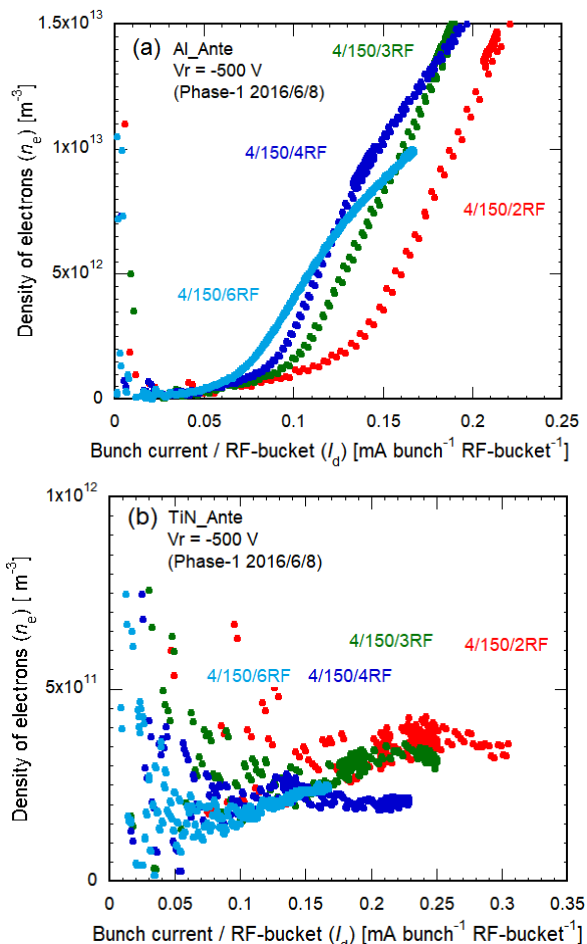


Figure 6: Measured densities of electrons ( $n_e$ ) in the test beam pipe at the region (a) without and (b) with TiN film coating as functions of the current linear density ( $I_d$ ) for various bunch fill patterns, where the grid voltage of the electron monitor was  $-500$  V.

On the other hand, the  $n_e$  in the TiN-coated region of the test beam pipe, in Fig. 6(b), was still slightly lower than  $I_{d,th}$  at the same  $I_d$ , although the values of  $n_e$  are scattered at a low  $I_d$  because of the measurement errors at small monitor currents. From these facts, it was suspected that the ECE was excited owing to the electrons at the Al-alloy region without coating in the ring.

It was finally found that this ECE was caused by the electrons in the Al-alloy bellows chambers without TiN film coating. They are 200 mm long and are located at an average of every 3 m around the ring as shown in Fig. 7(a). There are approximately 830 bellows chambers in total, and their total occupied length is  $\sim 5\%$  of the circumference of the ring. Therefore, if the  $n_e$  in the Al-alloy bellows chambers is 20 times that in the other TiN-coated regions, the ECE is likely to be excited.

To counteract the ECE, two units of permanent magnets (PM), where PM were attached to C-shaped iron plates (yokes), were placed at the top and bottom of each Al-alloy bellows chamber, as shown in Fig. 7(b). Each PM has a diameter of 30 mm, and the intensity of magnetic field at

the surface is approximately 850 G. A  $B_z$  of approximately 100 G is formed in most regions in the PM units, although the polarity reverses locally near the magnets.

After attaching the PM units to all Al-alloy bellows chambers, the non-linear increase in  $P/I$  relaxed substantially as shown in Fig. 4(a) ([with PM at bellows]), and the blow up of vertical beam size was not evident until  $I$  value reached approximately 800 mA, as shown in Fig. 4 (b) ([with PM at bellows]). Thus, the ECE was successfully suppressed by applying  $B_z$  using PM units on the Al-bellows chambers. The measurement of the vertical beam size for bunch fill patterns of 4/150/2RF, 4/150/3RF, 4/150/4RF and 4/150/6RF showed that the  $I_{d,th}$  shifted from 0.1–0.12 mA bunch $^{-1}$  RF-bucket $^{-1}$  to 0.18–0.2 mA bunch $^{-1}$  RF-bucket $^{-1}$ , as indicated in Fig. 5 (b).

At this point, approximately 90 % of the beam pipes in the LER have antechambers and TiN coating. It should be noted that the  $I_{d,th}$  is much higher than that in the case of the KEKB at the early stage [8], where most beam pipes were circular copper without any coating and solenoid windings. The  $I_{d,th}$  was approximately 0.04 mA RF-bucket $^{-1}$  at the early stage of the KEKB, as shown in Fig. 5(c). On the other hand, after applying PM units to Al-alloy bellows chambers in the SuperKEKB, the  $I_{d,th}$  is 0.18 – 0.2 mA bunch $^{-1}$  RF-bucket $^{-1}$  (Fig. 5 (b)), which is approximately 5 times that in the KEKB. This indicates that the antechambers and the TiN coating of the beam pipes effectively suppress the ECE.

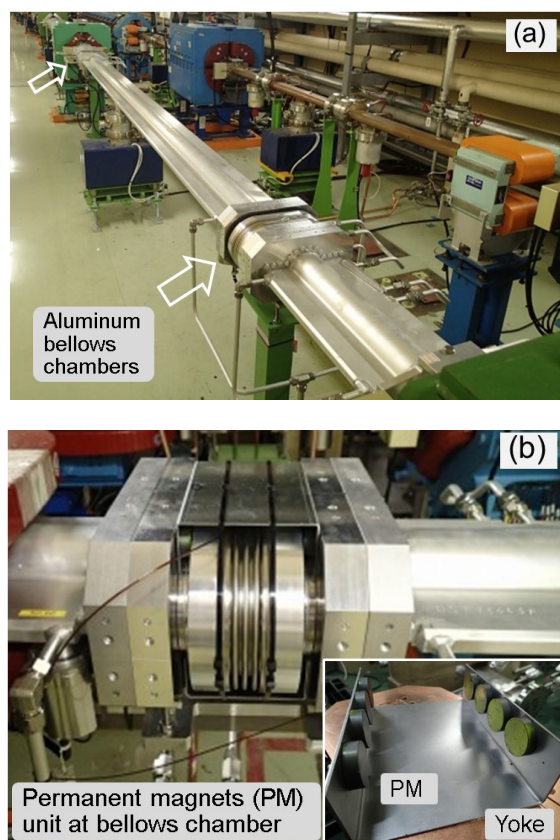


Figure 7: (a) Al-alloy bellows chambers in the LER, (b) PM and yokes (PM units) attached to them.

*ECE at higher beam current*

The ECE observed from an  $I$  value of approximately 600 mA caused by electrons in Al-alloy bellows chambers were successfully suppressed, as described above. However, as anticipated from Fig. 5(b), the ECE began to appear at an  $I$  value of approximately 900 mA at a bunch fill pattern of 1/1576/3.06RF. This  $I$  value corresponds to the  $I_c$  value of approximately 0.2 mA bunch<sup>-1</sup> RF-bucket<sup>-1</sup>. The blow up of vertical beam size reappeared at the same  $I$  as shown in Fig. 4 (b) ([with PM at bellows]). Furthermore, the  $n_e$  measured in the region with TiN film coating in the test beam pipe approached the value of  $n_{e,c}$  at the  $I_c$  of 0.2 mA bunch<sup>-1</sup> RF-bucket<sup>-1</sup> for 3RF-buckets and 2RF-buckets spacing as seen in Fig. 6(b). The growth rates of the transverse coupled bunch instabilities were measured using a bunch-by-bunch feedback system [9]. The modes caused by the electrons at the drift spaces were detected.

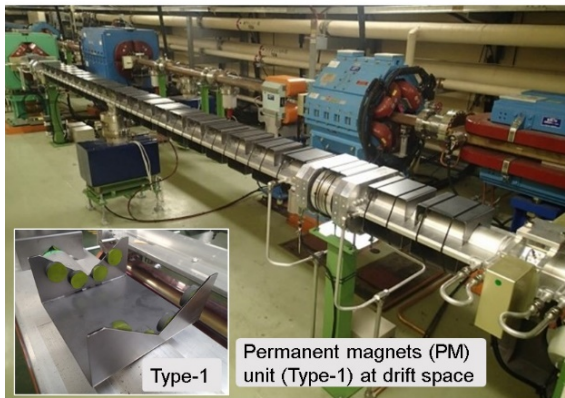


Figure 8: PM units (Type-1) attached to the beam pipes at drift spaces for test.

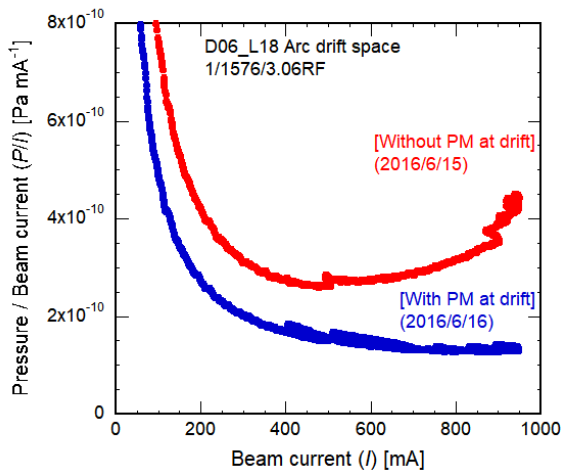


Figure 9: Behaviors of pressures in an arc section divided by the beam current ( $P/I$ ) against the beam current ( $I$ ) before and after attaching PM units to the beam pipes at drift spaces,

As a test, PM units similar to those used for the Al-alloy bellows chambers were attached to some beam pipes at drift spaces of approximately 20 m in an arc section (Fig. 8). The  $B_z$  value of over 60 G was obtained along the beam pipe, except for the polarity reversal points. After that, the  $P/I$  in this test region became flat and almost constant against  $I$ , as shown in Fig. 9 ([with PM at drift]). This meant that the ECE was excited by the electron cloud formed in the beam pipes with antechambers and TiN film coating at drift spaces.

The excitation of ECE meant that the countermeasures in Phase-1 commissioning were still insufficient. Additional countermeasures, that is, application of  $B_z$  by using PM units and solenoids to most drift spaces in the ring was required before starting the next commissioning.

Note here that the simulation of ECE indicates that the average value of the maximum SEY ( $\delta_{max}$ ) in the ring should be larger than 1.3 – 1.4 to excite ECE for the present condition of the LER. Here the ratio of the number of photoelectrons in the beam channel to the total number of those in the beam pipe was assumed to be 0.01 on the bases of the experimental result in KEKB [10]. On the other hand, the  $\delta_{max}$  measured in the laboratory was 0.9 – 1.2 at the estimated electron dose of  $5 \times 10^{-7}$  C mm<sup>-2</sup> [11], where the energy of incident electrons was 250 eV. The reason of the difference in the expected  $\delta_{max}$  has not been clarified. Some possibilities are; (1) The dose of electrons with sufficient energies is still low, that is, the aging of the surface is insufficient. However, little decrease in  $n_e$  at the region with TiN film coating was observed during Phase-2 commissioning relative to that in Phase-1 commissioning. (2) The pressure is still high in the beam pipe. It was found in an experiment at the laboratory that the maximum SEY was high if the samples were not baked and the pressure in the test chamber was high. (3) The number of photoelectrons is larger than expected in the beam channel of the real beam pipes with antechambers, due to scattering of photons and the vertical spread of SR. In any way, the investigations on this discrepancy in the  $\delta_{max}$  are in progress through simulations and experiments.

**ADDITIONAL COUNTERMEASURES**

As additional countermeasures against the ECE for the next Phase-2 commissioning, PM units and solenoids were attached to most of the beam pipes at drift spaces in LER. The PM units with iron yokes (Type-1 unit), similar to those used for Al-alloy bellows chambers, were placed in series around the beam pipe as shown in Fig. 10(a), which produced a  $B_z$  of approximately 60 G. A simulation by the code CLOUDLAND [12] showed that the  $n_e$  around the beam orbit reduced to approximately 1/10<sup>th</sup> of the  $n_{e,th}$  even for the designed beam parameters, as shown in Figs. 11 (a) and (b). However, the Type-1 unit cannot be used near electromagnets, such as quadrupole and sextupole magnets, because the iron yokes affect their magnetic field. Therefore, another type of PM units (Type-2 unit), which consists of Al-alloy cylinders with permanent magnets

inside and Al-alloy supports, was placed close to the electromagnets, as also shown in Fig. 10(a). The  $B_z$  inside the Type-2 unit was approximately 100 G. For the beam pipes that had been used since the KEKB era, solenoid windings were revived as shown in Fig. 10(b) [8]. Before starting Phase-2 commissioning, approximately 86% of the drift spaces (approximately 2 km) was covered with a  $B_z$  higher than approximately 20 G. Note that a simulation indicated that the  $n_e$  around the beam orbit in a  $B_z$  value higher than 10 G is lower than  $1 \times 10^{11} \text{ m}^{-3}$  even for the designed beam parameters.

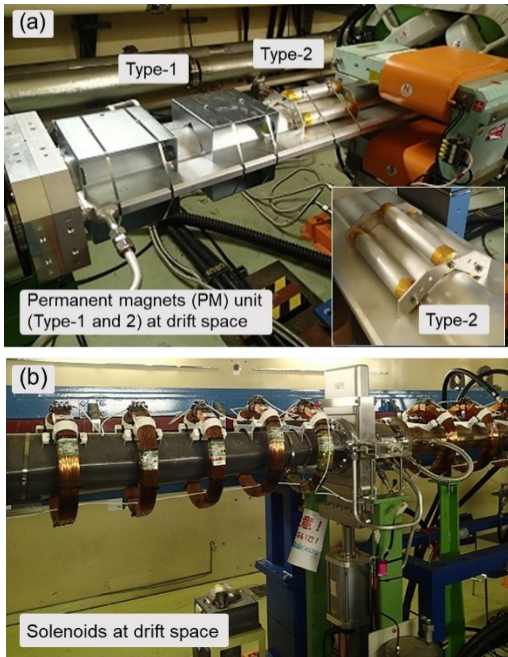


Figure 10: (a) Type-1 and Type-2 units and (b) solenoids at drift spaces.

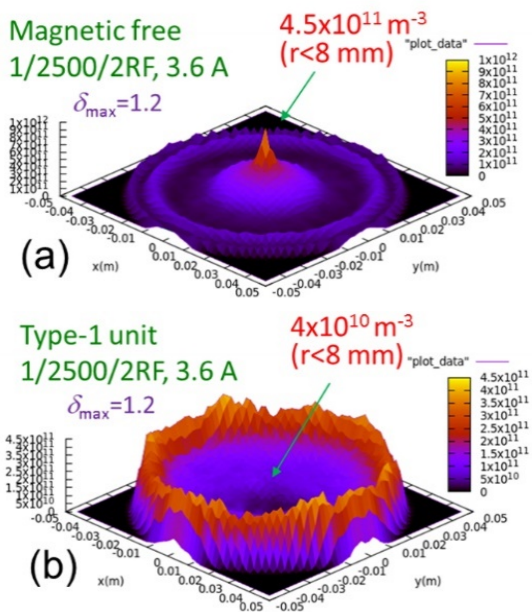


Figure 11: Density of electrons ( $n_e$ ) in a beam pipe (a) without magnetic field and (b) with Type-1 PM units calculated

by CLOUDLAND simulation code for a beam current of 3.6A at a bunch fill pattern of 1/2500/2RF.

### ECE IN PHASE-2 COMMISSIONING

The Phase-2 commissioning started in March 2018. The vertical beam sizes and the  $P/I$  were measured at the end of May as in the case during Phase-1.

Figure 12 shows the behavior of  $P/I$  at arc sections against  $I$ , for a bunch fill pattern of 2 RF-buckets spacings during Phase-1 and Phase-2 commissioning. As shown in Fig. 12, the  $P/I$  increased with  $I$  when the  $I$  value was higher than 300 mA in the case of Phase-1. On the other hand, the  $P/I$  is almost constant against  $I$  in the case of Phase-2 commissioning. This indicated less multipactoring of electrons. Note here that the  $P$  itself decreased in Phase-2 commissioning when compared to that in Phase-1 commissioning due to vacuum scrubbing [13].

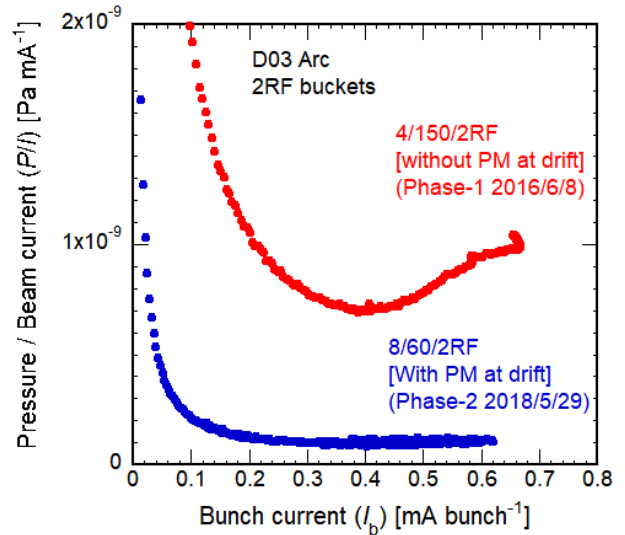


Figure 12: Behaviors of pressures at an arc section divided by the beam current ( $P/I$ ) against the bunch current ( $I_{\text{bunch}}$ ) in Phase-1 and Phase-2 commissioning (May 2018).

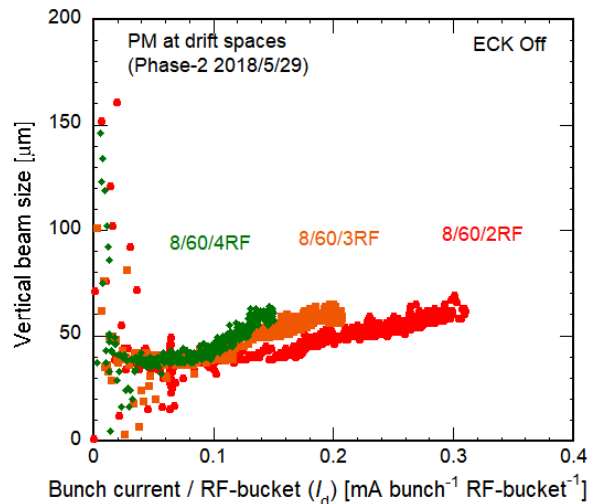


Figure 13: Vertical beam sizes as a function of current linear density ( $I_d$ ) for several bunch fill patterns during Phase-2 commissioning (May 2018).

Figure 13 shows the dependence of the vertical beam size on  $I_d$  for bunch fill patterns of 4/120/2RF, 4/120/3RF and 4/120/4RF. As shown in Fig. 13, the blow up was not observed until the  $I_d$  value of  $0.3 \text{ mA bunch}^{-1} \text{ RF-bucket}^{-1}$ . The  $I_{d,th}$  increased by at least 1.5 times when compared to the case of Phase-1 commissioning (Fig. 5(b)).

The modes and growth rates of the transverse coupled bunch instabilities were measured and analysed again. The modes caused by the electrons at near the inner wall trapped by  $B_z$  was observed, instead of the modes caused by the electrons in drift spaces. Furthermore, the growth rates were much slower than those measured during Phase-1 commissioning.

On the other hand, the measured  $n_e$  in the test beam pipe at the region with TiN film coating without Bz did not change from that observed in Phase-1 commissioning.

From these observations, it can be concluded that the additional countermeasures, i.e. a  $B_z$  generated by PM units and solenoids at drift spaces, contributed towards suppressing the ECE in Phase-2 commissioning.

## SUMMARY

The ECE was observed in the SuperKEKB LER during Phase-1 commissioning. The ECE due to Al-alloy bellows chambers was successfully suppressed by applying PM units which produced a  $B_z$  of several ten gauss in the bellows chambers. The ECE due to beam pipes at drift spaces, however, was still observed at higher current regions, although the beam pipes had antechambers and TiN film coating as countermeasures against ECE. The antechambers and TiN film coating seemed to be functioning to some extent, but further countermeasures were required for the next commissioning. As additional countermeasures, two types of PM units and solenoids were prepared for beam pipes at drift spaces before Phase-2 commissioning. The Phase-2 commissioning started on March 2018. The experiment at the end of May 2018 found that the  $I_{d,th}$  increased by at least 1.5 times when compared to that in Phase-1 commissioning. The non-linear increase in  $P/I$  with an increase in  $I$  also disappeared. The  $B_z$  for the beam pipes at drift spaces functioned well with regards to suppressing ECE. Further studies on the ECE are planned at higher beam currents. The re-evaluation of the effectiveness of antechambers and TiN film coating is also planned to check whether they are functioning as expected to explain the discrepancy between the  $\delta_{max}$  estimated in the ring and that obtained in the laboratory.

## ACKNOWLEDGEMENTS

The authors would like to thank all the staff of the KEKB accelerator division for their cooperation and continuous encouragement during the commissioning phase.

## REFERENCES

- [1] Y. Ohnishi, "Report on SuperKEKB phase 2 commissioning," in Proc. IPAC'18, Vancouver, Canada, April 29 – May 4, 2018, pp. 1–5.
- [2] K. Ohmi and F. Zimmermann, "Head-Tail Instability Caused by Electron Clouds in Positron Storage Rings," Phys. Rev. Lett. 85, p. 3821, 2000.
- [3] Y. Susaki et al., "Electron cloud instability in SuperKEKB low energy ring", in Proc. IPAC'10, Kyoto, May 23–28, 2010, pp.1545–1547.
- [4] Y. Suetsugu et al., "Results and problems in the construction phase of the SuperKEKB vacuum system," J. Vac. Sci. Technol. A, 34, p. 021605, 2016.
- [5] K. Kanazawa et al., "Measurement of the electron cloud density around the beam," in Proc. PAC'05, Knoxville, USA, May 16–20, 1995, pp. 1054–1056.
- [6] Y. Suetsugu et al., "Achievements and problems in the first commissioning of SuperKEKB vacuum system," J. Vac. Sci. Technol. A, 35, p. 03E103, 2017.
- [7] Y. Suetsugu et al., "First Commissioning of the SuperKEKB Vacuum System," Phys. Rev. Accel. Beams, 19, p. 121001, 2016.
- [8] H. Fukuma et al., "Status of Solenoid System to Suppress the Electron Cloud Effects at the KEKB", AIP Conference Proceedings 642, 2002, pp.357–359.
- [9] K. Ohmi, et al., "Electron cloud studies in SuperKEKB phase I commissioning," in Proc. IPAC2017, Copenhagen, Denmark, May 14–19, 2017, pp. 3104–3106.
- [10] Y. Suetsugu *et al.*, "R&D of copper beam duct with antechamber scheme for high current accelerators," Nucl. Instrum. Method Phys. Res. A, 538, p. 206, 2005.
- [11] K. Shibata *et al.*, "Development of TiN coating system for beam ducts of KEK B-factory," in Proc. EPAC'08, Genoa, Italy, June 23–27, 2008, pp. 1700–1702.
- [12] L. Wang *et al.*, "A perfect electrode to suppress secondary electrons inside the magnets," in Proc. EPAC 2006, Edinburgh, Scotland, June 26 – 30, 2006, pp.1489–1491.
- [13] Y. Suetsugu *et al.*, "Beam scrubbing of beam pipes during the first commissioning of SuperKEKB," Appl. Surface Sci., 432, p. 347, 2018.